CHALMERS

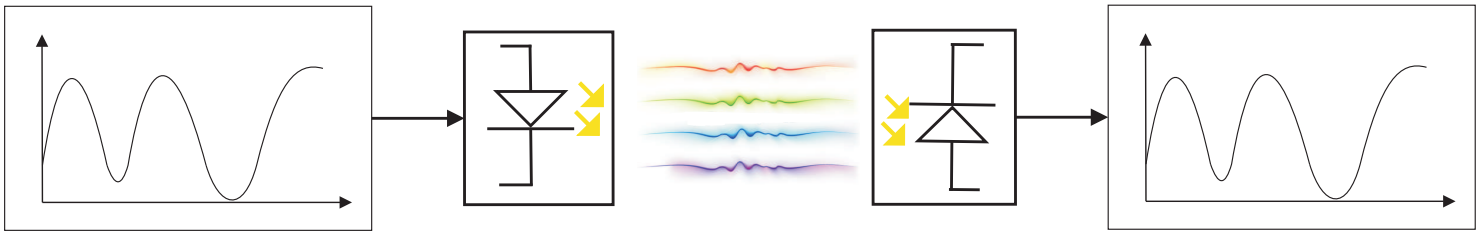

Bandlimited Power-Efficient Signaling and Pulse Design for Intensity Modulation

Cristian B. Czegledi

Communication Systems Group
Department of Signals and Systems
Chalmers University of Technology
Gothenburg, Sweden 2013

Czegledi, Cristian B.
Bandlimited Power-Efficient Signaling and Pulse Design for Intensity Modulation

Department of Signals and Systems
Technical Report No. EX045/2013

Communication Systems Group
Department of Signals and Systems
Chalmers University of Technology
SE-41296 Gothenburg, Sweden
Telephone: + 46 (0)31-772 1000

This thesis has been prepared using LaTeX.

Front Cover: A schematic of an intensity-modulation direct-detection optical communication system.

Abstract

With the increasing requirement of multimedia content, internet service providers have to spread more optical fiber in the network, build more data-centers and storage area networks, and offer high capacity wireless solutions. In long-haul fiber optical links, coherent transceivers are used, which provide high data rates for many users. In contrast, short-haul connections, known as intensity-modulation direct-detection (IM/DD) systems, often use noncoherent low-cost transceivers. Such systems are very sensitive to the transmitted optical power, both peak and average optical powers are strictly limited for safety and power-consumption considerations, and nonnegativity constraints are imposed on the transmitted optical signal.

In this report, new methods for power-efficient intersymbol interference-free transmission over the bandlimited IM/DD channel are proposed. A new bias signal is found and added to the transmitted signal to make it nonnegative. The new bias is time-varying and provides a more power-efficient transmission than the previously considered constant bias. In order to further improve the power efficiency, two approaches of designing new Nyquist and root-Nyquist pulses are presented. The first method lies in forming the pulse in the time domain, while pulse shaping in the frequency domain is used as an alternative approach. Analytical expressions for the asymptotic power efficiency and symbol error rate of the proposed schemes are derived and evaluated. At a spectral efficiency of 1 b/s/Hz and using on-off keying modulation, the proposed schemes outperform the squared-sinc pulse shaping, which is the previously most power-efficient known format, by 0.628 dB in asymptotic power efficiency.

KEYWORDS: Fiber-optical communications, free-space optical communications, direct detection, intensity modulation, strictly bandlimited signaling.

Preface

This report is the result of conducting a one-year 60 credit thesis work which is the requirement for obtaining Master of Science degree. This work is an extended version of C. B. Czegledi, M. R. Khanzadi, and E. Agrell, "Bandlimited Power-Efficient Signaling and Pulse Design for Intensity Modulation", a journal article manuscript in preparation for submission, which in turn is an extended version of C. B. Czegledi, M. R. Khanzadi, and E. Agrell, "Bandlimited Power-Efficient Signaling for Intensity Modulation", a submitted paper to Conference on Optical Fiber Communications (OFC), San Francisco, California, USA, March 2014.

November 6, 2013
Cristian B. Czegledi

Acknowledgments

First of all, it gives me great pleasure in acknowledging the support of my supervisor Prof. Erik Agrell. I would like to thank him for offering me this opportunity, his patience, motivation, enthusiasm, and constructive suggestions during this research work.

Assistance provided by M. Reza Khanzadi is greatly appreciated, his willingness to give his time so generously has been very much respected.

In addition, I would like to express my appreciation to all the people at the Department of Signals and Systems, for a very pleasant study experience in Gothenburg during the past two years.

Last but not least, my gratitude goes to my friends and family. Thank you for your help and support.

Gothenburg, November 6, 2013

Cristian B. Czegledi

CONTENTS

Acronyms

APE	Asymptotic Power Efficiency
AWGN	Additive White Gaussian Noise
BER	Bit Error Rate
BTN	Better Than Nyquist
DC	Direct-Current
IM/DD	Intensity-Modulation Direct-Detection
ISI	Intersymbol Interference
OOK	On-Off Keying
LED	Light-Emitting Diode
MF	Matched Filter
PAM	Pulse Amplitude Modulation
PCHI	Piecewise Cubic Hermite Interpolation
PL	Parametric Linear
RC	Raised-Cosine
S2	Squared-Sinc
SNR	Signal-to-Noise Ratio
VCSEL	Vertical-Cavity Surface-Emitting Laser

1 Introduction

Nowadays modern world requires a massive data transportation to satisfy a large number of users, who demand more multimedia content such as video and voice. This requires higher data transfer rate capabilities than ever. To satisfy this huge demand, internet service providers have to spread optical fiber deeper in the network, build more data-centers and storage area networks, and offer high capacity wireless solutions.

1.1 Optical communications

Optical communication dates since antiquity, mentioned by Homer in *Iliad*, when the Greeks used fire signaling to send messages while conquering Troy, approximately 1200 BC. The very early precedent of the modern optical communication was created by Alexander Graham Bell and Charles Sumner Tainter in 1880, called *Photophone* (Bouchet *et al.* 2010). The idea was to replace electrical wires with beams of light and on June 3, 1880, the first wireless optical phone conversation took place. Soon, the electromagnetic radiation was discovered by Hertz and many scientists and researchers focused their work on it. In the late 1950s, the laser was discovered (Agrawal 2005) and the today's optical communication was born. The first reliable optical guide environment was silica-glass fibers, proposed in (Kao and Hockham 1966).

Today's links using optical carriers vary from transoceanic distances to several meters. The long-haul optical connections provide the backbone for various types of networks worldwide, at high data rates. Such links are using coherent transceivers, where the information is encoded on both amplitude and phase of the transmitted signal, in both polarizations. As opposed to long-haul optical links, where

the deploying costs are shared among many users, the short-haul optical links are more cost sensitive. Examples of such connections are optical interconnections in high-performance computing centers, data-centers, storage area networks (Randel *et al.* 2008, Molin *et al.* 2011), and diffuse indoor wireless optical links (Hranilovic 2005*b*, Barry 1994). To reduce the overall costs of such transmissions, low-complexity and cheap optical hardware, e.g., noncoherent transceivers, are often used. These include vertical-cavity surface-emitting lasers (VCSELs), laser diodes, or light-emitting diodes (LEDs) used at the transmitter (denoted as Light source in Fig. 1.1-top), and photodetectors at the receiver (shown as Photodetector in Fig. 1.1-top) (Barry 1994, Ch. 1), (Westbergh *et al.* 2009). Usually for additional cost reductions, multimode fibers are employed. Due to their larger cores, compared to the single-mode fibers, a higher tolerance to alignment impairments in the connectors can be achieved, which reduces the installation costs.

In contrast to coherent systems, in a noncoherent optical link, only the intensity of the optical transmitted signal carries the useful information. Such optical connections are known as intesity-modulation direct-detection (IM/DD) systems.

1.2 Intensity-Modulation Direct-Detection Systems

In an IM/DD system, intensity modulation is obtained by varying the bias current of the light source at the transmitter, e.g., VCSEL or LED, which produces an optical waveform. This is observed at the receiver by direct detection, i.e., the photodetector will produce an electrical current proportional to the received optical power. The IM/DD systems can be used with optical amplifiers, for long-haul and metropolitan links, and without amplifiers for short-range connections.

A practical IM/DD system without amplification can be modeled as a baseband additive white Gaussian noise (AWGN) channel, shown in the bottom part of Fig. 1.1, imposing certain restrictions on the transmitted signal (Barry 1994, Ch. 5). First, the transmitted signal must be nonnegative, since only the intensity of the transmit-

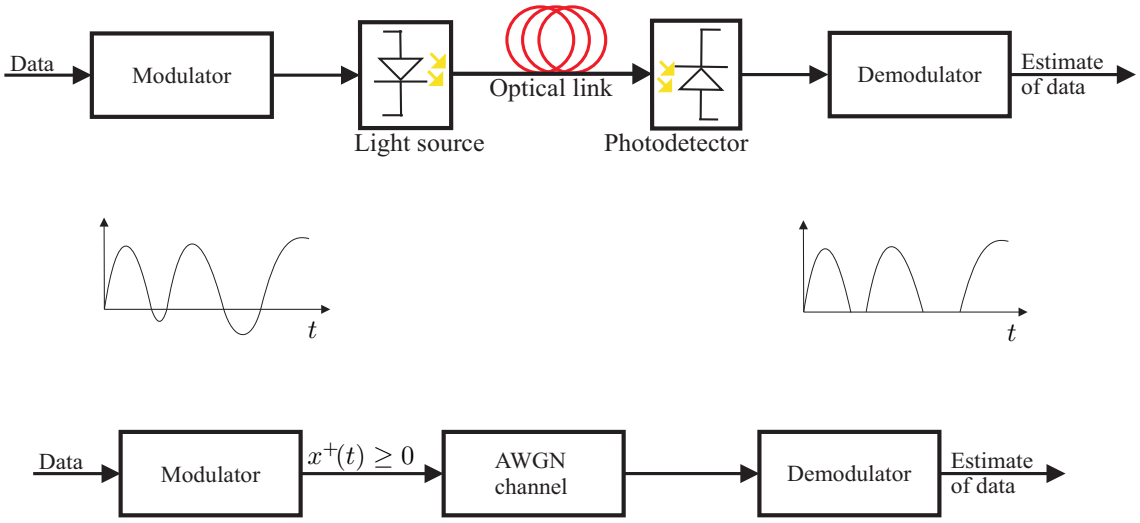

Figure 1.1. Passband transceiver of an IM/DD system without amplification (top). The clipping effect on the negative parts of the transmitted waveform (middle). The equivalent baseband model with nonnegativity constraint on the transmitted signal $x^+(t)$ (bottom).

ted optical waveform conveys information through the channel. Any negative part of the transmitted signal will be clipped, causing distortions (see Fig. 1.1). Second, due to safety regulations and power-consumption purposes, the average and peak optical powers have to be within certain limitations (Barry 1994, Ch. 5), (Hranilovic 2005*b*, Ch. 2).

In addition to the previous constraints, in this thesis only bandlimited intersymbol interference (ISI) free transmissions are studied. Bandlimitted transmission is considered to avoid distortions caused by low-cost optoelectronic devices and multipath distortion in indoor wireless optical links (Barry 1994). Moreover, it prevents interchannel interference in wavelength-division multiplexing transmission schemes. Additionally by considering only ISI-free transmissions, the receiver does not require equalization, which is necessary when ISI is allowed. Therefore, low-complex and low-cost receivers can be designed for such a transmission.

Such a system was investigated for the first time in (Hranilovic 2005*a*). Pulse amplitude modulation (PAM) schemes were designed using bandlimited ISI-free nonnegative Nyquist pulses, such as the squared-sinc (S2) pulse, at half the Nyquist rate. It was also shown that nonnegative bandlimited ISI-free root-Nyquist pulses

do not exist. As an extension, new nonnegative Nyquist pulses were introduced in (Hranilovic 2007), which provide a trade-off between the required optical power and the required bandwidth, that spans from half the Nyquist rate to the Nyquist rate.

A new modulation scheme for the bandlimited ISI-free IM/DD systems was proposed in (Tavan *et al.* 2012), where a direct-current (DC) bias signal is added to the transmitted waveform in order to make the signal nonnegative. This approach has benefits in terms of bandwidth, by enabling transmissions below half the Nyquist rate, and it also allows the use of root-Nyquist pulses. At the moment, there is still no modulation scheme having a better power efficiency at half the Nyquist rate than the scheme proposed in (Hranilovic 2005*a*), which uses the S2 pulse.

1.3 Contributions

In this report, design of bandlimited ISI-free IM/DD systems is investigated by presenting a new, more power-efficient signaling scheme, and two methods to obtain new pulses shapes, which further increase the optical power efficiency. The new scheme consists of a new bias signal, which is time-varying, different from the one previously proposed. The design of new pulse shapes, in the first method, is done in the time domain, and in the second approach, new pulses are obtained in the frequency domain. For the first time, the presented modulation schemes are more power-efficient than the previously best known signaling, which is based on S2 pulse, at a bandwidth equal to half the Nyquist rate.

1.4 Organization

The remainder of the report is organized as follows. Chapter 2 presents the system model. In Chapter 3, the proposed bias signal is presented and the considered performance measure, i.e., asymptotic power efficiency, is introduced. In Chapter 4,

the study optimizes the power efficiency by considering different pulse shapes. First, known pulses from the literature are investigated, then new methods for designing new pulses are proposed. In Chapter 5, the performance of proposed methods are evaluated. Finally, in Chapter 6, conclusions on the contributions are provided.

2 System Model

In this section, an IM/DD system is introduced, along with the imposed conditions from Sec. 1 on the transmitted signal. An IM/DD system without amplification can be modeled as a baseband AWGN channel, imposing certain restrictions on the transmitted signal (Barry 1994, Ch. 5). Fig. 2.1 shows the model of a IM/DD system, including a transmitter, a channel, and a receiver.

The transmitted nonnegative intensity is constructed as a modified PAM signal

$$x^{+}(t) = A(f(t) + \sum_{k=-\infty}^{\infty} a_k p(t - kT)), \tag{2.1}$$

where A is a positive power scaling factor, a_k is the k^{th} transmitted symbol uniformly draw from a finite one-dimensional constellation $\mathscr{C}$, T is the symbol time, and $p(t)$ is an arbitrary pulse shape of bandwidth $B \leq 1/T$. The nonnegativity constraint is satisfied by adding a proper signal bias $f(t)$ to the transmitted PAM signal.

The received signal is

$$y(t) = x^{+}(t) + n(t), \tag{2.2}$$

where $n(t)$ is zero mean AWGN with double-sided power spectral density $N_0/2$.

At the receiver, the exact same bias, $f(t)$, which is added at the transmitter, is subtracted from the received signal $y(t)$, making the rest of the receiver a conventional PAM demodulator.

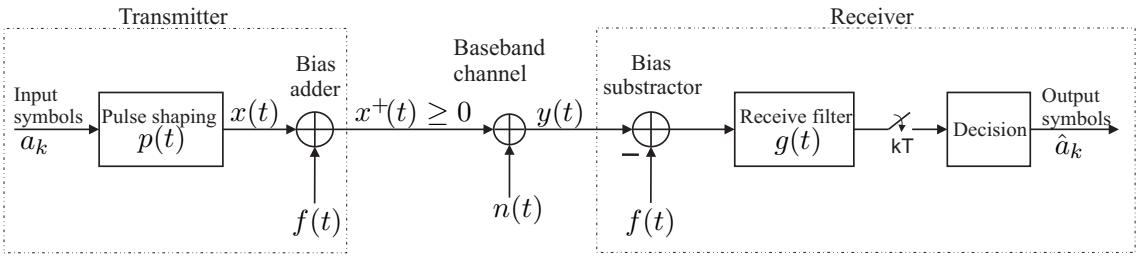

Figure 2.1. Baseband IM/DD system model

2.1 Average and Peak Optical Power

According to (Barry 1994, Ch. 5), (Hranilovic 2007, Ch. 2), the average optical power is computed as the average amplitude of $x^+(t)$

$$P_{\text{opt}} = \frac{1}{T}\int_0^T \mathbb{E}\{x^+(t)\}\mathrm{d}t, \tag{2.3}$$

where $\mathbb{E}\{\cdot\}$ denotes statistical expectation.

The peak optical power is

$$\begin{aligned} P_{\max} &= \max(x^+(t)) \\ &= \max\left(A(f(t) + \sum_{k=-\infty}^{\infty} a_k p(t-kT))\right), \end{aligned} \tag{2.4}$$

for all sequences ..., a_{-1}, a_0, a_1, a_2, ..., and for all $t \in \mathbb{R}$, where $\mathbb{R}$ denotes the set of real numbers.

For safety and power-consumption considerations, the average and peak optical powers have to be within certain limitations.

2.2 ISI-free and Bandwidth Constraints

To fulfill the bandwidth restriction on $x^+(t)$, the pulse shape $p(t)$, used at the transmitter is always bandlimited, $B \leq 1/T$. The ISI-free condition is achieved by considering two scenarios. One when the receiver's filter $g(t)$ is flat in the band of interest and it is called sampling receiver, and the matched-filter (MF) receiver, where the receive filter $g(t)$ is matched to the transmitter's pulse shape $p(t)$.

To fulfill the ISI-free condition in the first case, the pulse $p(t)$ has to satisfy the

Nyquist criterion (Proakis and Salehi 2008, Eq. (9.2-12))

$$p(nT) = \begin{cases} 1 & n = 0 \\ & \\ 0 & n \neq 0 \end{cases}, \tag{2.5}$$

or its Fourier transform $P(f)$ must satisfy the Nyquist criterion in the frequency domain (Proakis and Salehi 2008, Eq. (9.2-13))

$$\sum_{m=-\infty}^{\infty} P(f + m/T) = T. \tag{2.6}$$

In the MF receiver scenario, the receive filter is matched to the transmitter filter. In order to meet the ISI-free constraint at the output signal after the MF, a root-Nyquist pulse $P_{\text{RN}}(t)$ can be used at the transmitter, which can be obtained from a Nyquist pulse by applying (Proakis and Salehi 2008, Eq. (9.2-29))

$$P(f) = P_{\text{RN}}(f) = \sqrt{|P_{\text{N}}(f)|}e^{-j2\pi f t_0}, \tag{2.7}$$

where $P_{\text{N}}(f)$ is the frequency response of the Nyquist pulse, $j = \sqrt{-1}$ is the imaginary quantity, and t_0 is a delay to allow nonsymmetric pulses and to ensure physical realizability of the filter. Considering an ideal channel, i.e., a channel with a normalized flat response in the band of interest, to match the receive filter to the transmitter's filter, its frequency response is $G(f) = P^*(f)$, where $(\cdot)^*$ denotes the complex conjugate.

3 The Bias

In this section, the proposed bias signal is introduced, which guarantees the non-negativity of the transmitted signal. The procedure of finding a power-efficient modulation scheme can be formulated as an optimization problem, where the optical power efficiency is maximized by finding the optimal bias signal $f(t)$, as well as the design of an optimal constellation $\mathscr{C}$, and the pulse shape $p(t)$. However, in this thesis, previously known constellations are used and the focus is on the design of $f(t)$ and $p(t)$.

3.1 The Bias Expression

To fulfill the nonnegativity constraint, the bias signal is added to the PAM signal in (2.1). The bias signal $f(t)$ can be any waveform, as long as it is strictly bandlimited and achieves the nonnegativity of the transmitted signal.

For all $t \in \mathbb{R}$ and all sequences $\ldots, a_{-1}, a_0, a_1, a_2, \ldots$, (2.1) can be rewritten as

$$x^{+}(t) = A\left(f(t) + \sum_{k=-\infty}^{\infty} (a_k - L)\, p(t - kT) + L \sum_{k=-\infty}^{\infty} p(t - kT) \right), \tag{3.1}$$

where $L = (\overline{c} + \underline{c})/2$ is the midpoint of the constellation, $\overline{c} = \max_{c \in \mathscr{C}} c$, and $\underline{c} = \min_{c \in \mathscr{C}} c$.

According to (Tavan *et al.* 2012, Corollary 2), for a bandlimited $B \leq 1/T$ pulse $p(t)$

$$\sum_{k=-\infty}^{\infty} p(t - kT) = \frac{P(0)}{T}, \tag{3.2}$$

which is a constant independent of t.

Using (3.2), (3.1) can be rewritten as

$$x^{+}(t) = A\left(f(t) + \sum_{k=-\infty}^{\infty} (a_k - L)\, p(t - kT) + \frac{LP(0)}{T} \right). \tag{3.3}$$

In the right hand side of (3.3), the last term is constant and the required bias $f(t)$ depends only on the summation term. The worst case scenario is when all the terms in the summation are minimum (the most negative value of each term), requiring the largest bias. The term can be at its minimum in two cases. First, when $(a_k - L)$ is maximum, i.e., $(\overline{c} - L)$, and $p(t - kT) < 0$, or when $(a_k - L)$ is minimum, i.e., $(\underline{c} - L)$, and $p(t - kT) > 0$. Both cases are the same because $(\overline{c} - L) = -(\underline{c} - L)$. Thus (3.3) can be bounded as

$$x^{+}(t) \geq A\left(f(t) + (\underline{c} - L) \sum_{k=-\infty}^{\infty} |p(t - kT)| + \frac{LP(0)}{T} \right), \tag{3.4}$$

for any t.

The choice of $f(t)$ depends only on the summation $\sum_{k=-\infty}^{\infty} |p(t - kT)|$, which is a time-varying, periodic function with period equal to T. Therefore, the choice of $f(t)$ is also a time-varying, periodic function with the period equal to T/z, where $z \in \mathbb{N}_{\neq 0}$ can be any nonzero natural number. According to (Phillips *et al.* 2008, p. 171), a periodic function with the period equal to T/z can be decomposed into its Fourier series

$$f(t) = \mu_0 + \sum_{k=1}^{\infty} \mu_k \cos\left(\frac{2\pi k z t}{T} + \phi_k \right), \tag{3.5}$$

where μ_0 is a constant and μ_k and ϕ_k are the amplitude and the phase, respectively, of the k^{th} cosine component.

The bias signal has to be a waveform which is strictly bandlimited, $B \leq 1/T$, to satisfy the condition imposed in Sec. 1. Therefore, the optimum form of $f(t)$,

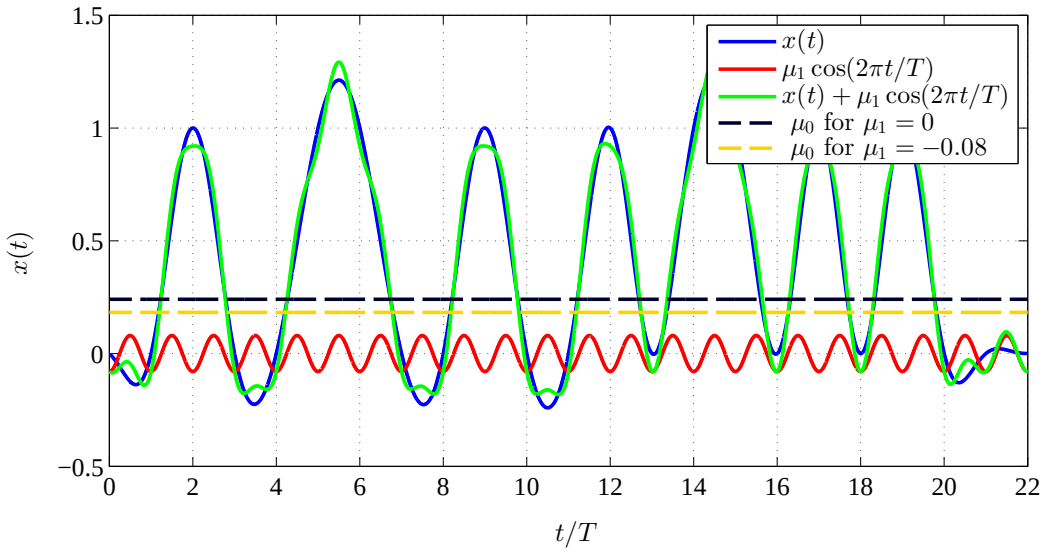

Figure 3.1. A PAM signal, $x(t)$, using $\mathscr{C} = \{0, 1\}$ and the RC pulse with $\alpha = 0.5$ is plotted. The required DC bias in (Tavan *et al.* 2012) is $\mu_0 = -\min x(t) = 0.241$ for $\mu_1 = 0$; using the optimal cosine bias, $\mu_1 = -0.08$ and $\phi = 0$, the required DC bias becomes $\mu_0 = 0.182$.

considered here is

$$f(t) = \mu_0 + \mu_1 \cos\left(\frac{2\pi t}{T} + \phi\right), \tag{3.6}$$

where to satisfy the bandwidth limitation only the first term of the summation in (3.5) is considered and $z = 1$. For the sake of notation simplicity $\phi = \phi_1$. For any given μ_1 and ϕ, the DC component μ_0 can be chosen to ensure $x^+(t) \geq 0$.

From the average optical power perspective, the cosine component of the bias does not require extra power since its integral is zero in (2.3). The extra power is consumed only by the DC bias. However, compared to (Tavan *et al.* 2012), the transmission is more power-efficient because less DC bias is required after adding the cosine term.

By replacing (3.6) in (2.1), the transmitted signal becomes

$$x^+(t) = A\left(\mu_0 + \mu_1 \cos\left(\frac{2\pi t}{T} + \phi\right) + \sum_{k=-\infty}^{\infty} a_k p(t - kT)\right), \tag{3.7}$$

where setting $\mu_1 = 0$, (3.7) becomes the same as (Tavan *et al.* 2012, Eq. (1)).

The effect of the bias on the transmitted signal is plotted in Fig. 3.1, where a PAM signal is formed using the raised-cosine (RC) pulse with the roll-off factor $\alpha = 0.5$, (see Sec. 4.1), and $\mathscr{C} = \{0, 1\}$. The required DC bias in (Tavan *et al.* 2012), μ_0, for $\mu_1 = 0$, is decreased by adding the cosine term to the transmitted signal.

The cost of adding the time-variable bias is an increased bandwidth. Without adding $f(t)$, the required bandwidth is equal to the bandwidth of the pulse $p(t)$, i.e., $B \leq 1/T$, whereas after adding the bias, the required bandwidth becomes $B = 1/T$. It must be noted that the receiver does not need any extra synchronization for the time-varying bias, since the cosine term has the same period as the symbol clock.

3.2 Bias Coefficients

In the previous section, the optimal form of the bias was proposed. In this section, the bias parameters μ_0, μ_1, and ϕ are optimized to maximize the optical power efficiency.

From (3.4) and (3.6), the optimal value of μ_0 as a function of μ_1 and ϕ can be written as

$$\mu_0 = \max_{0 \leq t < T} \left((\overline{c} - L) \sum_{k=-\infty}^{\infty} |p(t - kT)| - \mu_1 \cos\left(\frac{2\pi t}{T} + \phi\right)\right) - \frac{LP(0)}{T}. \tag{3.8}$$

As mentioned earlier, the cosine component of the bias does not have any effect on the optical power. However, any choice of μ_1 and ϕ affects the optimal value of μ_0. Hence, μ_0 is minimized, which maximizes the optical power efficiency over μ_1 and ϕ

$$\mu_0 = \min_{\substack{0 \leq \phi < 2\pi \\ \mu_1 \in \mathbb{R}}} \max_{0 \leq t < T} \left((\overline{c} - L) \sum_{k=-\infty}^{\infty} |p(t - kT)| - \mu_1 \cos\left(\frac{2\pi t}{T} + \phi\right)\right) - \frac{LP(0)}{T}. \tag{3.9}$$

From (3.9, it can be seen that the DC bias μ_0, depends on the constellation $\mathscr{C}$,

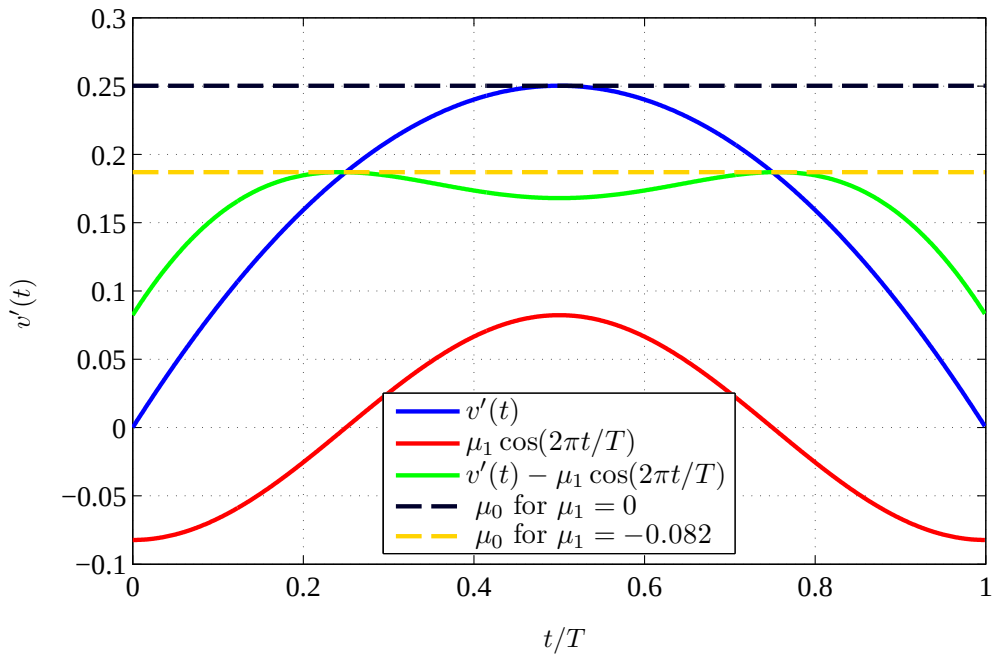

Figure 3.2. The function $v'(t)$ for the RC pulse $p(t)$, with $\alpha = 0.5$ and $\mathscr{C} = \{0, 1\}$ is shown. The DC bias μ_0 is decreased from 0.25 to 0.187 by using the cosine bias ($\mu_1 = -0.082$, $\phi = 0$).

the pulse shape $p(t)$, the amplitude μ_1, and the phase ϕ of the variable bias and not on the instantaneous transmitted symbols. Solving this equation analytically is impossible, but using a numerical computing software it can be easily solved.

For notational simplicity, let $v(t) = (\overline{c} - L) \sum_{k=-\infty}^{\infty} |p(t - kT)|$ and $v'(t) = v(t) - LP(0)/T$, both can be encountered in (3.9).

Fig. 3.2 shows $v'(t)$, for a RC pulse with $\alpha = 0.5$, and using $\mathscr{C} = \{0, 1\}$, as a function of time t, and the required DC bias, first for $\mu_1 = 0$ (Tavan *et al.* 2012), and in the second case for the optimal pair (μ_1, ϕ). The values of μ_0 and μ_1 are different from the ones shown in Fig. 3.1, because in Fig. 3.2, the worst-case scenario is considered, while in the example in Fig. 3.1 this was not the case.

3.3 Power Efficiency

The average optical power can be computed by substituting (3.7) in (2.3), which yields

$$\begin{aligned} P_{\text{opt}} &= \frac{1}{T}\int_0^T A\left(\mu_0 + \mu_1 \cos\left(\frac{2\pi t}{T} + \phi\right) + \mathbb{E}\{a_k\}\sum_{k=-\infty}^{\infty} p(t-kT)\right)\mathrm{d}t \\ &= A\left(\mu_0 + \mathbb{E}\{a_k\}\bar{p}\right), \end{aligned} \tag{3.10}$$

where

$$\bar{p} = \frac{1}{T}\int_0^T p(t)\mathrm{d}t = \frac{P(0)}{T}. \tag{3.11}$$

By substituting the bias expression in (2.4), the peak optical power can be computed as

$$P_{\max} = \max\left(A\left(\mu_0 + \mu_1 \cos\left(\frac{2\pi t}{T} + \phi\right) + \sum_{k=-\infty}^{\infty}(a_k - L)\,p(t-kT) + \frac{LP(0)}{T}\right)\right), \tag{3.12}$$

for all t. Replacing the expression of μ_0 and considering the worst case scenario as in (3.4), $P_{\max}$ becomes

$$P_{\max} = A\left(\max_{0\le t<T}\left(v(t) - \mu_1\cos\left(\frac{2\pi t}{T} + \phi\right)\right) + \max_{0\le t<T}\left(v(t) + \mu_1\cos\left(\frac{2\pi t}{T} + \phi\right)\right)\right). \tag{3.13}$$

Theorem 1. *The peak optical power, P_{max}, of the transmitted signal $x^+(t)$ defined in (3.7) is bounded by*

$$2A\max_{0\le t<T} v(t) \le P_{\max} \le 2A(\max_{0\le t<T} v(t) + |\mu_1|). \tag{3.14}$$

Proof. Both inequalities can be easily proven by starting from the fundamental

inequality

$$\max(f(t)+g(t)) \leq \max(f(t)) + \max(g(t)). \tag{3.15}$$

The first inequality can be proved by replacing $f(t) = v(t) - \mu_1 \cos(2\pi t/T + \phi)$ and $g(t) = v(t) + \mu_1 \cos(2\pi t/T + \phi)$ in (3.15). The second inequality can be proved using

$$\begin{aligned} \max(v(t) \pm \mu_1 \cos(2\pi t/T + \phi)) &\leq \max(v(t)) + \max(\pm\mu_1 \cos(2\pi t/T + \phi)) \\ &= \max(v(t)) + |\mu_1| \,. \end{aligned} \tag{3.16}$$

□

The lower bound in (3.14) is the peak optical power required in (Tavan *et al.* 2012) and can be obtained by setting $\mu_1 = 0$ in (3.13).

In contrast to the average optical power, the peak optical power does not depend on the DC bias, μ_0, whereas it only depends on the cosine bias parameters, μ_1 and ϕ. Minimizing the average optical power by minimizing the DC bias in (3.9) does not guarantee the minimum peak optical power. A trade-off between average and peak optical power can be obtained by optimizing (3.9) and (3.13) over μ_0, μ_1 and ϕ at the same time. However, the objective in this report is to minimize the average optical power.

Fig. 3.3 shows the trade-off between $P_{\max}$ and P_{opt} and their corresponding minimum values computed for the RC pulse with $\alpha = 0.5$ (left) and for the $\mathfrak{R}$(RC) pulse (see Sec. 4.1) with $\alpha = 1$ (right) using $\mathscr{C} = \{0, 1\}$. In the first case, the minimum average optical power is obtained when $\mu_1 = -0.08$, while the minimum peak optical power is obtained when $-0.05 \leq \mu_1 \leq 0.05$. If the minimum peak optical power is desired, there is no reason to set $\mu_1 \neq -0.05$; at the this point, keeping $P_{\max}$ minimum, P_{opt} is also minimum. In the flat region of the curve (red part), $P_{\max}$ is at its lower bound in Theorem 1, where the sum of the two maximization in (3.13) is equal to $2 \max v(t)$. For the figure in the right, the minimum values for both average and peak optical powers are achieved for $\mu_1 = 0.137$.

The achievable optical power gains of the proposed method are computed in terms

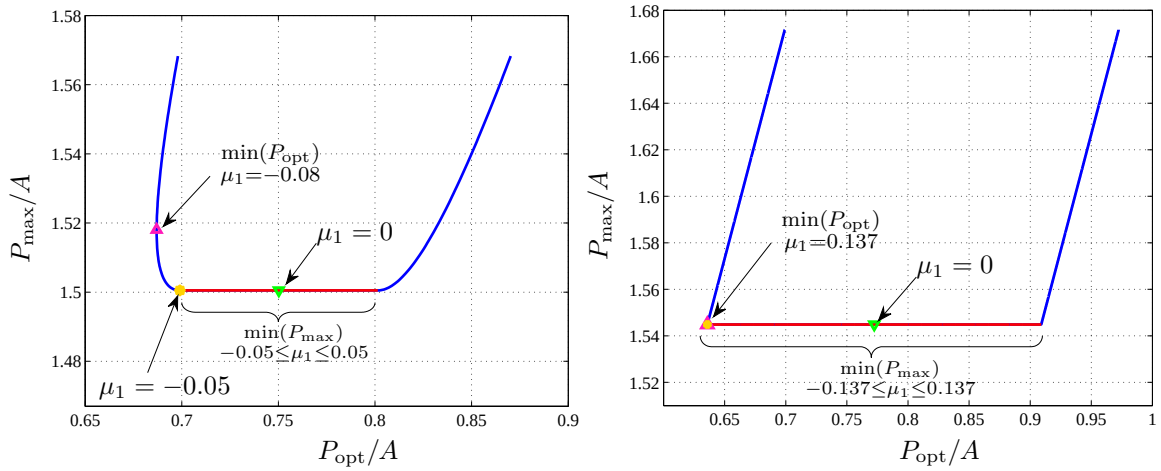

Figure 3.3. The peak optical power is plotted as a function of the average optical power for the RC pulse with $\alpha = 0.5$ (left) and for the $\mathfrak{R}$(RC) pulse with $\alpha = 1$ (right) and $\mathscr{C} = \{0, 1\}$.

of the asymptotic power efficiency (APE), defined as

$$\text{APE} = \frac{P_{\text{opt}}^{\text{ref}}}{P_{\text{opt}}}, \tag{3.17}$$

where $P_{\text{opt}}^{\text{ref}}$ is the average optical power required by the benchmark signaling (Hranilovic 2005*a*), based on the S2 pulse using $\mathscr{C} = \{0, 1\}$ and a sampling receiver, as in (Barry 1994, Ch. 5), (Kahn and Barry 1997), and P_{opt} is the average optical power required by the proposed method. The S2 pulse does not require any bias signal and offers the most power-efficient signaling at the same bandwidth as the proposed signaling, $B = 1/T$, which leads to a fair comparison.

3.4 M-PAM Analysis

In the previous sections, the relations are valid for any choice of one-dimensional constellation, while in this section, the APE is calculated for any M-ary PAM (M-PAM) constellation. According to (Tavan *et al.* 2012, Theorem 3), the performance of a constellation $\mathscr{C}$ does not change if all the constellation points are shifted with a constant offset. Without loss of generality, in this thesis the constellation $\mathscr{C}$ is chosen to be a nonnegative M-PAM constellation defined as $\mathscr{C} = \{0, 1, 2, ..., M-1\}$,

with the parameters $\underline{c} = 0$, $\overline{c} = M - 1$, $L = \mathbb{E}\{a_k\} = (M-1)/2$, and $\Delta a = 1$, where Δa is the minimum distance of the constellation.

The scaling factor A can be computed as a function of the symbol error rate P_e, in both sampling and MF receiver scenarios.

3.4.1 Sampling Receiver

In this case, using the same principles as in (Tavan *et al.* 2012), the parameter A becomes

$$A = \frac{2}{\Delta a \; p(0)} Q^{-1}\left(P_e \frac{M}{2(M-1)}\right) \sqrt{N_0 B}, \tag{3.18}$$

where M is the cardinality of the constellation, B is the required bandwidth, and $Q(\cdot)$ is the Gaussian Q-function defined as

$$Q(x) = \frac{1}{2\pi} \int_x^\infty \exp\left(\frac{-x^2}{2}\right) \mathrm{d}x, \tag{3.19}$$

and $Q(\cdot)^{-1}$ means its inverse.

Replacing (3.18) in (3.10), the average optical transmitted power becomes

$$P_{\text{opt}} = Q^{-1}\left(P_e \frac{M}{2(M-1)}\right) \sqrt{N_0 B} \frac{2\mu_0 + (M-1)\bar{p}}{p(0)}. \tag{3.20}$$

The average optical power required by the benchmark signaling, using (3.20), is

$$P_{\text{opt}}^{\text{ref}} = Q^{-1}\left(P_e\right) \sqrt{N_0 B_{\text{ref}}}, \tag{3.21}$$

where $B_{\text{ref}} = 1/T$.

Substituting (3.20) and (3.21) in (3.17) and taking the limit $P_e \to 0$, since the interest is in the asymptotical power efficiency, the APE expression in the case of

sampling receiver is

$$\text{APE} = \sqrt{\frac{B_{\text{ref}}}{B}} \frac{p(0)}{2\mu_0 + (M-1)\bar{p}}. \tag{3.22}$$

3.4.2 Matched Filter Receiver

The APE for the MF receiver can be computed by taking similar steps as in the sampling receiver case. In this case, A becomes (Tavan *et al.* 2012)

$$A = Q^{-1}\left(P_e \frac{M}{2(M-1)}\right) \frac{1}{\Delta a} \sqrt{\frac{2N_0}{E_p}}, \tag{3.23}$$

where $E_p = \int_{-\infty}^{\infty} p(t)^2 \mathrm{d}t$ (Tavan *et al.* 2012).

Using (3.23), the average optical power becomes

$$P_{\text{opt}} = Q^{-1}\left(P_e \frac{M}{2(M-1)}\right) \sqrt{\frac{2N_0}{E_p}} \left(\mu_0 + \frac{(M-1)\bar{p}}{2}\right). \tag{3.24}$$

After substituting (3.21) and (3.24) in (3.17) and letting $P_e \rightarrow 0$, the APE becomes

$$\text{APE} = \sqrt{2B_{\text{ref}}E_p} \frac{1}{2\mu_0 + (M-1)\bar{p}}. \tag{3.25}$$

4 Pulse Design

In the previous section, the optimal optical power efficiency, i.e., APE, was found by optimizing only the bias signal $f(t)$. In this section, the optimization is reformulated by simultaneous optimization of the pulse shape $p(t)$ and the bias signal $f(t)$. The APE can be maximized by choosing the pulse shape $p(t)$, the cosine-bias coefficients μ_1 and ϕ, and the DC bias μ_0, while keeping the rest of the systems parameters such as the constellation $\mathscr{C}$ constant.

For convenience, the operator $\mathfrak{R}(\cdot)$ is defined, which converts a Nyquist pulse into its corresponding root-Nyquist pulse using (2.7), with both input and output being in the time domain, as

$$p_{\text{RN}}(t) = \mathfrak{R}(p_{\text{N}}(t)) = \mathscr{F}^{-1}(\sqrt{|\mathscr{F}(p_{\text{N}}(t))|}), \tag{4.1}$$

where $\mathscr{F}(\cdot)$ denotes the Fourier transform, $\mathscr{F}(\cdot)^{-1}$ means its inverse, $p_{\text{N}}(t)$ is the initial Nyquist pulse, and $p_{\text{RN}}(t)$ is the resultant root-Nyquist pulse.

The following sections present different choices of the pulse shape $p(t)$, used in the optimization process to find the scheme with the maximum achievable APE. In Sec. 4.1, pulses already known in the literature are introduced, and in Sec. 4.2 and 4.3 new pulses are designed, first by combining pulses in the time domain, and then the pulses are numerically constructed in the frequency domain.

4.1 Known Pulses

In this thesis, the most common Nyquist pulses known in the literature are analyzed, such as the well-known RC pulse (Proakis and Salehi 2008, Eq. (9.2-27))

$$\mathrm{RC}(t) = \begin{cases} \frac{\pi}{4}\mathrm{sinc}\left(\frac{t}{T}\right) & t = \pm\frac{T}{2\alpha} \\ \mathrm{sinc}\left(\frac{t}{T}\right)\frac{\cos(\frac{\pi\alpha t}{T})}{1-\left(\frac{2\alpha t}{T}\right)^2} & \text{otherwise} \end{cases}, \tag{4.2}$$

where $\mathrm{sinc}(x) = \sin(\pi x)/\pi x$ and the excess bandwidth is controlled by the roll-off factor $\alpha \in [0, 1]$. For $\alpha > 0$, the tails of the pulse decay as $1/|t^3|$.

The next studied pulse is the "better than Nyquist" (BTN) pulse (Beaulieu *et al.* 2001)

$$\mathrm{BTN}(t) = \mathrm{sinc}\left(\frac{t}{T}\right)\frac{\frac{2\pi\alpha t}{T\ln 2}\sin(\frac{\pi\alpha t}{T}) + 2\cos(\frac{\pi\alpha t}{T}) - 1}{(\frac{\pi\alpha t}{T\ln 2})^2 + 1}, \tag{4.3}$$

which has a slower decaying rate, $1/t^2$, compared to the RC pulse.

The parametric linear (PL) pulse of the first-order, presented in (Beaulieu and Damen 2004), is

$$\mathrm{PL}(t) = \mathrm{sinc}\left(\frac{t}{T}\right)\mathrm{sinc}\left(\frac{\alpha t}{T}\right), \tag{4.4}$$

which also decays as $1/t^2$ and is less sensitive to timing jitter than the RC pulse.

The first-order Xia pulse defined in (Xia 1997, Tan and Beaulieu 2004) is

$$\mathrm{Xia}(t) = \begin{cases} \frac{\pi}{2}\mathrm{sinc}\left(\frac{t}{T}\right) & t = -\frac{T}{2\alpha} \\ \mathrm{sinc}\left(\frac{t}{T}\right)\frac{\cos(\frac{\pi\alpha t}{T})}{\frac{2\alpha t}{T}+1} & \text{otherwise} \end{cases}. \tag{4.5}$$

It is ISI-free with or without matched filtering, satisfying both the Nyquist and root-Nyquist criteria at the same time. One of the main differences between Xia and the rest of the pulses is nonsymmetry in time domain. The Xia pulse has more energy for $t < 0$ than for $t > 0$ in the time domain.

None of the pulses presented above are nonnegative. They have a bandwidth equal

to $B = (1+\alpha)/2T$, and for $\alpha = 0$ they all result in the sinc pulse, which is an impractical waveform, since the summation in (3.9) diverges, requiring an infinite DC bias μ_0.

The S2 pulse, proposed in (Hranilovic 2005*a*) is nonnegative, ISI-free, and strictly bandlimited, defined as

$$\mathrm{S2}(t) = \mathrm{sinc}^2\left(\frac{t}{T}\right), \tag{4.6}$$

which satisfies the conditions by being a squared-Nyquist pulse and has a bandwidth $B = 1/T$. The S2 pulse is positive at any time t, hence does not require any bias signal.

In this study, the performance of each pulse with both sampling and MF receivers is analyzed. The $\mathfrak{R}(\cdot)$ operator is used to obtain root-Nyquist pulses, except the Xia pulse, which does not require any transformation since it is a Nyquist and a root-Nyquist pulse at the same time. As a side note, the well known root-raised cosine pulse is obtained by applying the $\mathfrak{R}(\cdot)$ operator on the RC pulse. From now on, in this thesis, when the performance of a pulse with the MF receiver is analyzed, the pulse is referred to as $\mathfrak{R}$(pulse), otherwise the $\mathfrak{R}(\cdot)$ notation is dropped. This implies that (4.1) is also applied, except the Xia pulse.

4.2 Composite Pulses

In this section, new pulses denoted as "composite pulses" are designed by linear combinations of the pulses introduced in the previous section. A composite pulse is the result of adding different Nyquist pulses in the time domain. The added pulses are required to have the same symbol time T. Therefore the outcome of the addition is a Nyquist pulse with the same symbol time. The employed pulses can be combined with different coefficients and different roll-off factors. For complexity

reasons, in this study only two pulses are combined to form a composite pulse

$$p(t,\alpha) = i_1 p_1(t,\alpha_1) + i_2 p_2(t,\alpha_2), \tag{4.7}$$

where $i_1, i_2 \in \mathbb{R}$ are the combining coefficients, $\alpha_1, \alpha_2 \in [0,1]$ are the roll-off factors, and p_1, p_2 are two arbitrary Nyquist pulses mentioned in Sec. 4.1, respectively. The roll-off factor of the obtained composite pulse $p(t,\alpha)$ is $\alpha = \max\{\alpha_1, \alpha_2\}$.

By optimizing among the $(i_1,\ i_2,\ \alpha_1,\ \alpha_2)$ parameters in (4.7), better pulses can be obtained, which are at least as good as the best pulse in the summation. A composite pulse can be used along with a sampling receiver. Moreover, its corresponding root-Nyquist pulse can be obtained using the $\mathfrak{R}(\cdot)$ operator and employed with an MF receiver.

4.3 Frequency-Shaped Pulses

In Sec. 5.2, new composite pulses are obtained in the time domain, while in this section, new pulses are constructed by optimizing them in the frequency domain.

A Nyquist pulse in the frequency domain, $P(f)$, has to satisfy (2.6). Accordingly, it can be designed as

$$P(f) = \begin{cases} \mathcal{Q}(f) & 0 \le f < \frac{1}{2T} \\ \frac{T}{2} & f = \frac{1}{2T} \\ T - \mathcal{Q}(\frac{1}{T} - f) & \frac{1}{2T} < f < \frac{1}{T} \\ 0 & f \ge \frac{1}{T} \end{cases}, \tag{4.8}$$

where $\mathcal{Q}(f)$ is a real-valued function with $T/2 \le \mathcal{Q}(f) \le T$. Hence, it is enough to know $\mathcal{Q}(f)$ in order to design a Nyquist pulse. To maximize the APE, new pulses are obtained by optimizing the $\mathcal{Q}(f)$ function using the Nelder-Mead algorithm

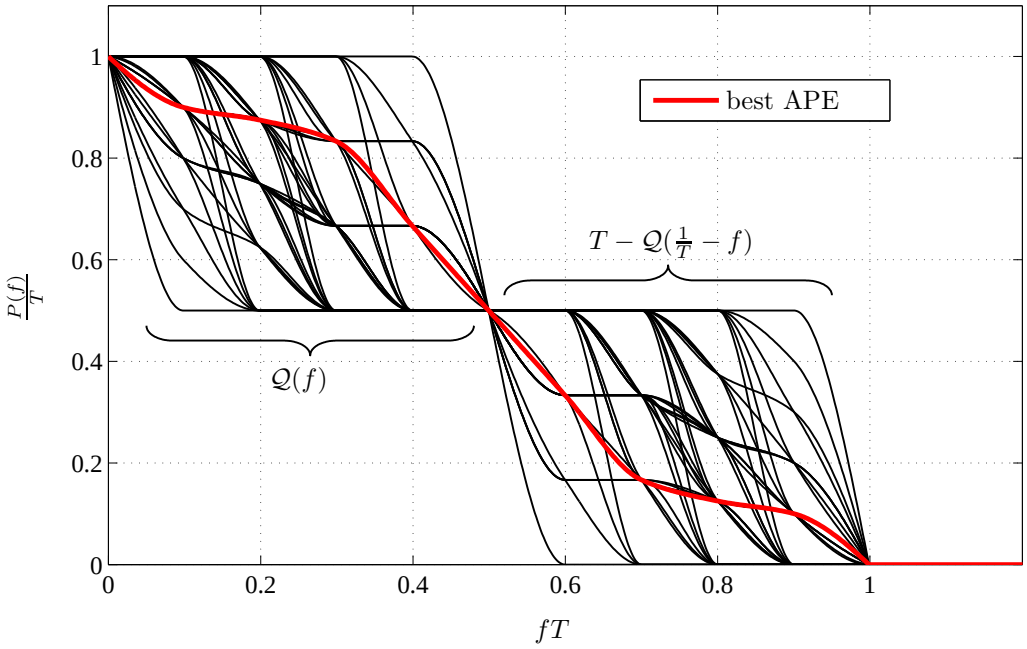

Figure 4.1. The Fourier transform $P(f)$ vs. frequency f of several pulses obtained during a low resolution grid search of $\mathcal{Q}(f)$. The red curve achieves the maximum APE out of this set of curves.

described in (Nelder and Mead 1965). The algorithm starts from an initial discrete shape of $\mathcal{Q}(f)$, with $\mathcal{N}$ equally spaced points from 0 to $1/2T$, and tries to converge to the optimum shape, such that the objective function, APE, is maximized.

In order to maximize the efficiency of the optimization, the input curve to the algorithm is chosen close to the optimal solution. Therefore, the starting values of $\mathcal{Q}(f)$ are determined using a grid search. For computation complexity reasons during the grid search, the frequency spectrum from 0 to $1/2T$ of $\mathcal{Q}(f)$ is discretized only into 6 equally spaced points. Two points are fixed, $\mathcal{Q}(0) = T$, $\mathcal{Q}(1/2T) = T/2$, and the remaining four points $\mathcal{Q}(i/10T)$ $i \in \{1, 2, 3, 4\}$ are varied within the interval $[T/2,\ T]$. The optimized pulse with the best APE is given as an input to the Nelder-Mead optimization algorithm, after it is upsampled to $\mathcal{N}$ points.

The upsampling of $\mathcal{Q}(f)$ is acquired using piecewise cubic Hermite interpolation (PCHI). Hence, the first derivative of $P(f)$ is continuous and consequently the obtained pulse shapes decay with at least $1/\left|t^3\right|$ in the time domain.

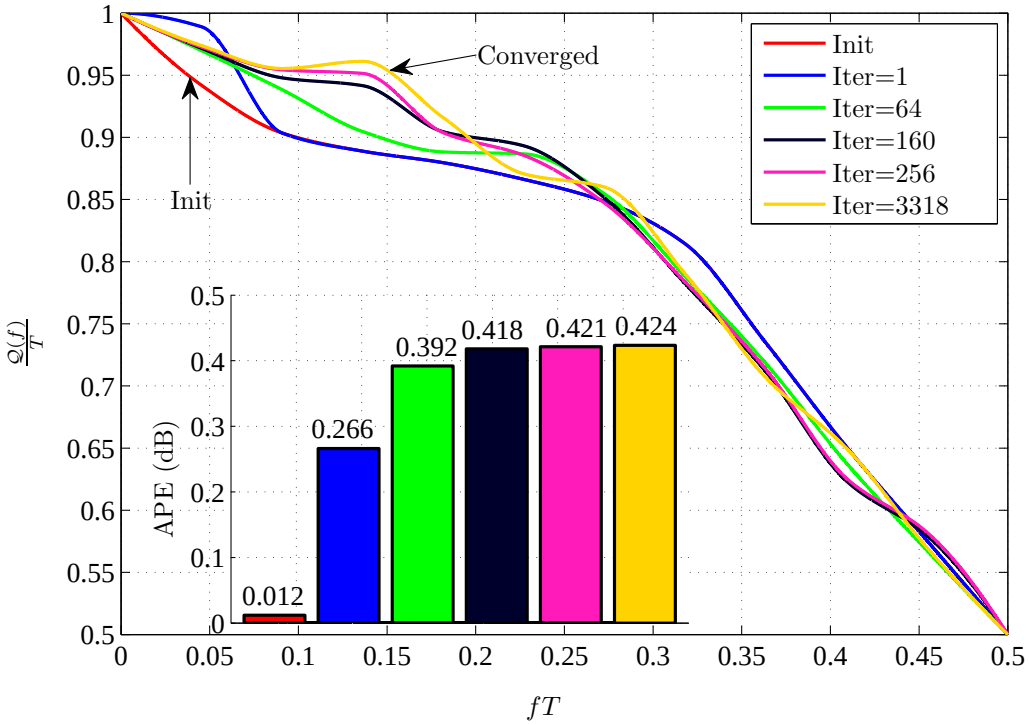

Figure 4.2. The optimization process of the curve with highest APE from Fig. 4.1 (red curve). Several intermediate steps are shown along the achieved APE values at each step. Between 256 and 3318 iterations, the changes in the APE and the shape are very small, which is the reason why no such curves are plotted.

Even though a grid search is performed before applying the Nelder-Mead algorithm, there is no guarantee that the output of the optimization reaches global maximum. The APE expression is not necessarily concave, and the algorithm can be trapped in one of the local maxima.

In Fig. 4.1, an example of a low-resolution grid search is shown along the curve having the maximum APE out of the presented set of curves. Fig. 4.2 shows the second stage of the APE optimization, which is a continuation of the result of the grid search from Fig. 4.1. The best curve from the grid search is upsampled to $\mathcal{N} = 12$ and input to the Nelder-Mead algorithm.

5 Results

In this section, the achievable performance gains of the proposed methods are investigated. In Sec. 5.1, the variable-bias signaling method is applied to previously known pulses, while in Sec. 5.2 and 5.3, further gains are achieved by designing new pulses specifically for the variable-bias signaling. For the sake of simplicity and without loss of generality, results obtained using $\mathscr{C} = \{0, 1\}$ are presented.

5.1 Known Pulses

In Fig. 5.1, the APE of the $\mathfrak{R}$(RC) pulse is presented as a function of the roll-off factor α and the amplitude of the variable bias μ_1. As mentioned in Sec. 3.1, the bandwidth of the variable bias is equal to $1/T$, therefore the required bandwidth B is equal to $1/T$, except for $\mu_1 = 0$, where $B = (1 + \alpha)/2T$. Using the variable bias, the maximum APE = 0.454 dB is reached at ($\alpha = 1,\ \mu_1 = 0.137,\ \phi = 0,\ \mu_0 = 0.136$), where 0.679 dB is gained in APE compared to pure DC bias with maximum APE = -0.225 dB at ($\alpha = 0.715,\ \mu_1 = 0,\ \phi = 0,\ \mu_0 = 0.244$), at a cost of an increased bandwidth. The variable bias, μ_1, decreases the required DC bias μ_0 and therefore less optical power (3.10) is required.

Fig. 5.2 shows the APE versus excess bandwidth α, for the pulses defined in Sec. 4.1, used with sampling or MF receiver. For any α, the APE is optimized over μ_0, μ_1, and ϕ. In general, the APE increases with α and achieves its maximum at $\alpha = 1$, except for $\mathfrak{R}$(PL) and $\mathfrak{R}$(BTN), where the APE reaches its maximum at $\alpha = 0.992$ and $\alpha = 0.976$, respectively. At $\alpha = 0$, each pulse becomes a sinc pulse, reaching the minimum APE, since the sinc pulse requires an infinite DC bias μ_0.

All the pulses, apart from Xia, are symmetric around the origin in the time domain, which is the reason why the optimum phase of the bias is $\phi = 0$. The Xia pulse

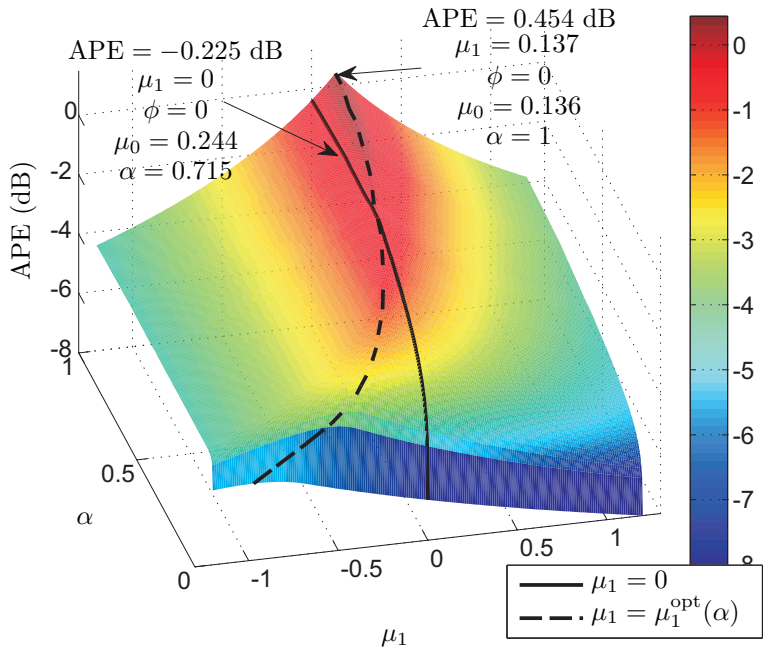

Figure 5.1. APE as a function of μ_1 and the roll-off factor α, for the $\mathfrak{R}$(RC) pulse. By setting $\mu_1 = 0$, the added bias becomes a pure DC bias and the obtained APE curve agrees with (Tavan *et al.* 2012). The dashed curve is obtained using the variable bias and for every value of α, the optimum μ_1 was used, $\mu_1^{\text{opt}}(\alpha)$. The improvement of the variable bias over the DC bias is 0.679 dB, reaching the maximum APE at $\alpha = 1$.

requires an optimum phase $\phi \neq 0$, except for $\alpha = 0$, where Xia becomes a pure sinc pulse.

In Fig. 5.2, it can also be observed that the MF receiver is more efficient than the sampling receiver for all α and all pulses. If only the DC bias μ_0 is used, $\mu_1 = 0$, the sampling receiver has a better performance (Tavan *et al.* 2012), and if no bias is used, $\mu_0 = \mu_1 = 0$, then there is no root-Nyquist pulse that can be used with an MF receiver (Hranilovic 2005*a*).

Theorem 2. *For $\alpha = 1$, the $\mathfrak{R}$(Xia) pulse is a shifted version of the $\mathfrak{R}$(RC) pulse by $T/4$.*

Proof. According to (Anderson 2005, Eq. (2.2-11)) the expression of the $\mathfrak{R}$(RC)

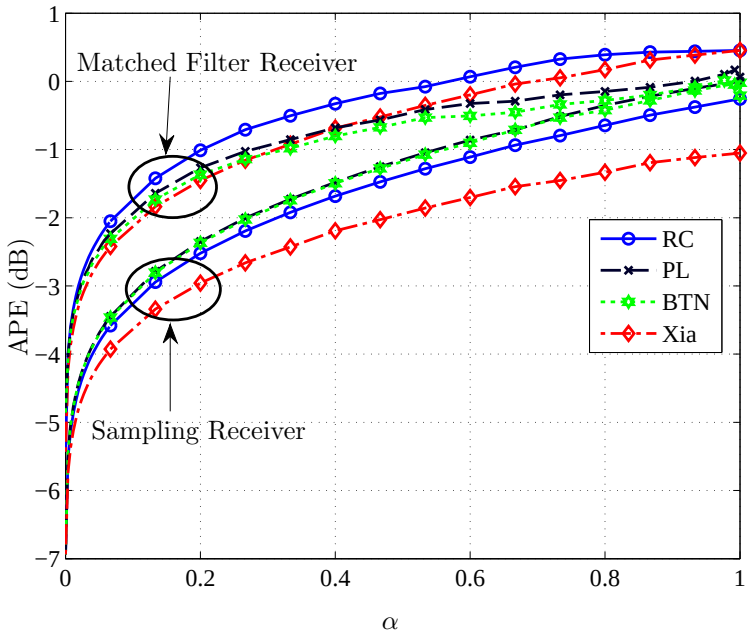

Figure 5.2. APE versus the roll-off factor α, for different pulses in both scenarios, using a sampling receiver and using an MF receiver, respectively. The best APE is obtained by $\mathfrak{R}$(RC) and $\mathfrak{R}$(Xia) at $\alpha = 1$ and is equal to 0.454 dB. The curve corresponding to the RC pulse with an MF receiver, i.e., $\mathfrak{R}$(RC), is the same curve as the $\mu_1 = \mu_1^{\text{opt}}(\alpha)$ (dashed) curve in Fig. 5.1.

pulse in the time domain is

$$\mathfrak{R}(\mathrm{RC}(t)) = \begin{cases} \frac{\alpha}{\sqrt{2}}\left(\left(1+\frac{2}{\pi}\right)\sin\left(\frac{\pi}{4\alpha}\right)+\left(1-\frac{2}{\pi}\right)\cos\left(\frac{\pi}{4\alpha}\right)\right) & t = \pm\frac{T}{4\alpha} \\ \frac{\sin\left(\frac{\pi(1-\alpha)t}{T}\right)+\frac{4\alpha t}{T}\cos\left(\frac{\pi(1+\alpha)t}{T}\right)}{\frac{\pi t}{T}\left(1-\left(\frac{4\alpha t}{T}\right)^2\right)} & \text{otherwise} \end{cases}, \tag{5.1}$$

which for $\alpha = 1$ becomes

$$\mathfrak{R}(\mathrm{RC}(t)) = \begin{cases} 1 & t = \pm\frac{T}{4} \\ \frac{4\cos\left(\frac{2\pi t}{T}\right)}{\pi\left(1-\left(\frac{4t}{T}\right)^2\right)} & \text{otherwise} \end{cases}. \tag{5.2}$$

On the other hand, the time expression of the $\mathfrak{R}$(Xia) pulse is (Tan and Beaulieu 2004, Eq. (3))

$$\mathfrak{R}(\mathrm{Xia}(t)) = \begin{cases} 1 & t = -\frac{T}{2\alpha} \\ \frac{\sin\left(\frac{\pi t}{T}\right)}{\frac{\pi t}{T}}\frac{\cos\left(\frac{\pi\alpha t}{T}\right)}{\frac{2\alpha t}{T}+1} & \text{otherwise} \end{cases}. \tag{5.3}$$

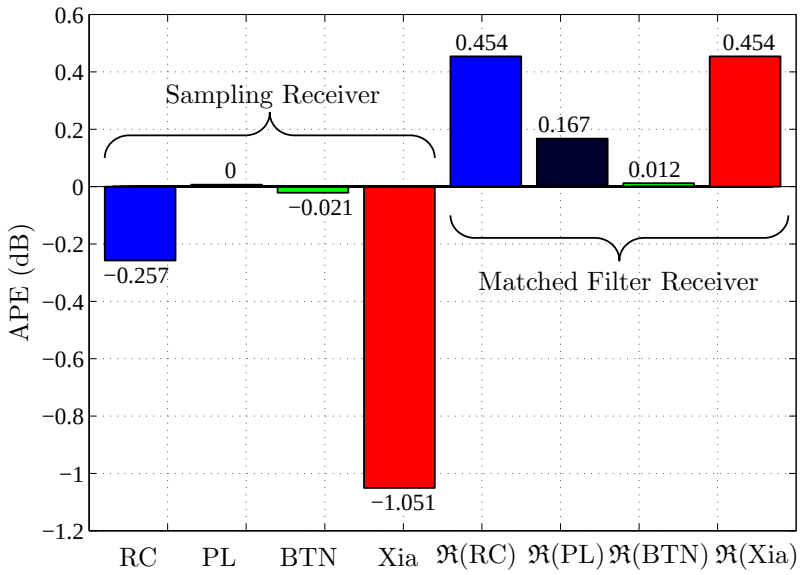

Figure 5.3. The maximum APE achieved by the pulses in Fig. 5.2. Most of the pulses result in the best APE when $\alpha = 1$, except $\mathfrak{R}$(PL) for which $\alpha = 0.992$ and $\mathfrak{R}$(BTN) for which $\alpha = 0.976$.

Setting $\alpha = 1$ and replacing t with $t = t - T/4$ in (5.3) yields

$$\begin{aligned}
\mathfrak{R}(\mathrm{Xia}(t - T/4)) &= \begin{cases} 1 & t - \frac{T}{4} = -\frac{T}{2} \\ \dfrac{\sin\left(\frac{\pi\left(t-\frac{T}{4}\right)}{T}\right)}{\frac{\pi\left(t-\frac{T}{4}\right)}{T}} \dfrac{\cos\left(\frac{\pi\left(t-\frac{T}{4}\right)}{T}\right)}{\frac{2\left(t-\frac{T}{4}\right)}{T}+1} & \text{otherwise} \end{cases} \\
&= \begin{cases} 1 & t = -\frac{T}{4} \\ \dfrac{\frac{1}{2}\sin\left(\frac{2\pi\left(t-\frac{T}{4}\right)}{T}\right)}{\pi\left(2\left(\frac{t}{T}\right)^2-\frac{1}{8}\right)} & \text{otherwise} \end{cases} \\
&= \begin{cases} 1 & t = -\frac{T}{4} \\ \dfrac{4\cos\left(\frac{2\pi t}{T}\right)}{\pi\left(1-\left(\frac{4t}{T}\right)^2\right)} & \text{otherwise} \end{cases},
\end{aligned} \tag{5.4}$$

which agrees with (5.2). □

Fig. 5.3 compares the maximum APE values obtained by the pulses shown in Fig. 5.2. The best APE is obtained simultaneously by $\mathfrak{R}$(RC) and $\mathfrak{R}$(Xia), due to the result of Theorem 2. For $\phi = \pi/2$ radians in case of using the Xia pulse, the same APE

Table 5.1. The achievable APE (dB) of the proposed signaling method for various pulses and their correspondent bias coefficients. The highlighted cells have the best APE.

	$f(t)$	RC	PL	BTN	Xia
Sampling receiver	μ_0	-0.277 $\mu_0 = 0.033$	0 $\mu_0 = 0$	-0.039 $\mu_0 = 0.005$	-1.893 $\mu_0 = 0.273$
	$\mu_0+\mu_1\cos(\frac{2\pi t}{T}+\phi)$	-0.257 $\mu_0 = 0.031$ $\mu_1 = 0.011$	0 $\mu_0 = 0$ $\mu_1 = 0$	-0.032 $\mu_0 = 0.004$ $\mu_1 = 0.004$	-1.051 $\mu_0 = 0.137$ $\mu_1 = 0.136$
			$\phi = 0$		$\phi = \pi/2$
Matched filter receiver	μ_0	-0.388 $\mu_0 = 0.273$	-0.771 $\mu_0 = 0.345$	-0.905 $\mu_0 = 0.371$	-0.388 $\mu_0 = 0.273$
	$\mu_0+\mu_1\cos(\frac{2\pi t}{T}+\phi)$	0.454 $\mu_0 = 0.137$ $\mu_1 = 0.136$	0.171 $\mu_0 = 0.180$ $\mu_1 = 0.166$	0.010 $\mu_0 = 0.205$ $\mu_1 = 0.169$	0.454 $\mu_0 = 0.137$ $\mu_1 = 0.136$
			$\phi = 0$		$\phi = \pi/2$

as for the $\mathfrak{R}$(RC) pulse is obtained.

Tab. 5.1 compares the best obtained APE for different pulses using the DC and variable bias signal, at $B = 1/T$. All the results are obtained for $\alpha = 1$, except PL, $\alpha = 0.992$, and BTN, $\alpha = 0.976$, both using MF receiver and variable bias.

5.2 Composite Pulses

In this section, the achievable APEs of the composite pulses presented in Sec. 4.2 are analyzed. The composite pulses are obtained by performing a grid search over the parameters in (4.7). The grid search varies $-1 \leq i_1, i_2 \leq 1$, which are the combining coefficients, with a step size of 1/191 and $0 \leq \alpha_1, \alpha_2 \leq 1$, which are the roll-off factors of the first and second pulse, with a step size of 1/21. The quartets $(i_1,\ i_2,\ \alpha_1,\ \alpha_2)$ which achieve the maximum APEs are shown in Tab. 5.2.

In Fig. 5.4, the achievable APEs obtained using the results from Tab. 5.2 and an

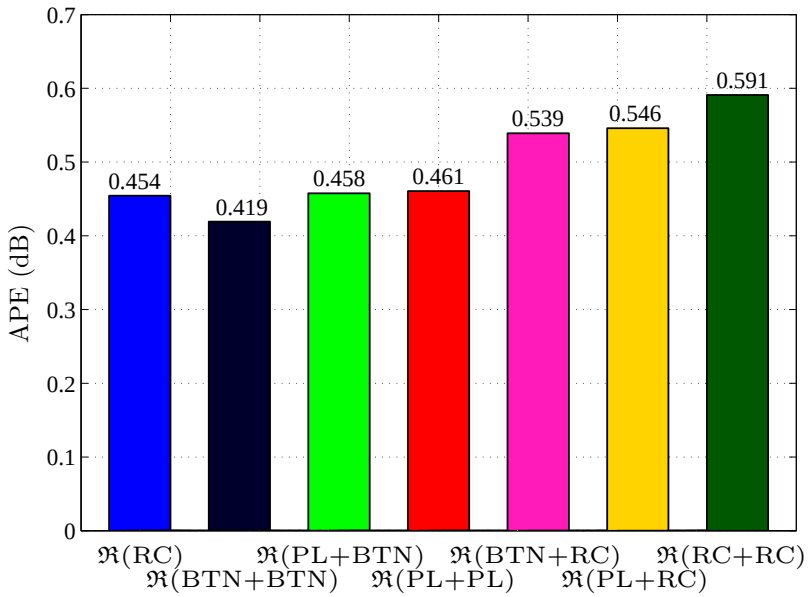

Figure 5.4. Maximum APE gains of pulses obtained as a summation of two known pluses.

Table 5.2. Composite Pulses Table

Pulse	i_1	α_1	i_2	α_2	APE (dB)
$\mathfrak{R}$(BTN+BTN)	0.4013	1	0.5987	0.4	0.419
$\mathfrak{R}$(PL+BTN)	3.5551	1	−2.5551	1	0.457
$\mathfrak{R}$(PL+PL)	0.4029	1	0.5971	0.45	0.461
$\mathfrak{R}$(BTN+RC)	0.0753	1	0.9247	0.8	0.539
$\mathfrak{R}$(PL+RC)	0.3958	0.4	0.6042	1	0.546
$\mathfrak{R}$(RC+RC)	0.3582	1	0.6418	0.65	0.591

MF receiver are compared against the best pulse from Sec. 5.1, the $\mathfrak{R}$(RC) pulse. In general, the composite pulses formed by using the RC pulse have higher APEs, where $\mathfrak{R}$(RC+RC) gives the best performance. As expected, the composite pulses containing RC can at least have the same APE as $\mathfrak{R}$(RC).

5.3 Frequency-Shaped Pulses

In this section, a numerically optimized pulse in the frequency domain from Sec. 4.3 is compared with the best pulses from the previous sections. The frequency-shaped pulse is obtained by the procedure described in Sec. 4.3, starting with a grid search on the discrete points of $\mathcal{Q}(f)$ in the frequency domain. The step size is $T/390$ for the frequency point at $\mathcal{Q}(1/10T)$, $19T/5100$ for the second frequency point at $\mathcal{Q}(1/5T)$, and $29T/5100$ for the last two frequency points at $\mathcal{Q}(3/10T)$ and $\mathcal{Q}(4/10T)$. A non-equal computational effort is used for the different frequency points because the APE quantity seems to be more sensitive to the changes in $\mathcal{Q}(f)$ in its first half of the frequency domain $[0,\ 1/4T]$, than changes in its second half $[1/4T,\ 1/2T]$. The shape of $\mathcal{Q}(f)$ which offers the maximum APE is further optimized using the Nelder-Mead algorithm to further increase the APE gain. The discrete frequency shape of $\mathcal{Q}(f)$ is upsampled using PCHI from the 6 points obtained during the grid search to $\mathcal{N}$ points, and then used as initial values of the Nelder-Mead algorithm.

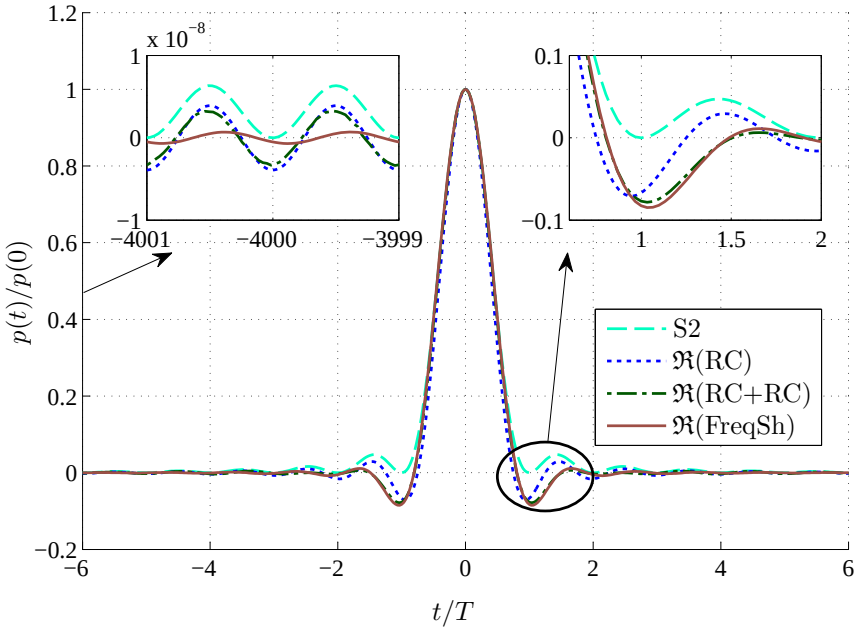

Figure 5.5. Several pulses are compared in the time domain. The decaying rate is visible in the top left subfigure and the main lobe is shown in the top right subfigure. The numerically optimized pulse, which provides the best performance, has the biggest side lobe and the best decaying rate.

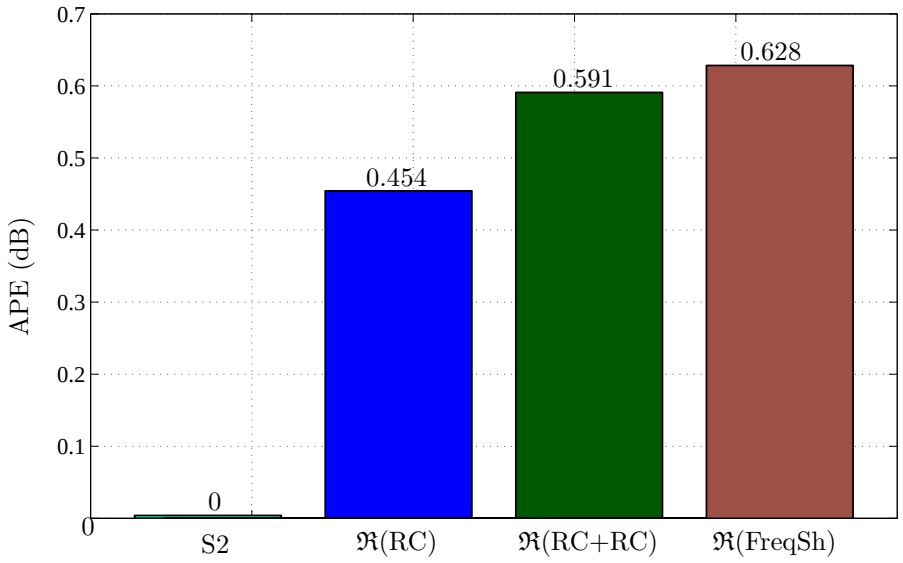

Figure 5.6. The achievable APE of the pulses shown in Fig. 5.5. The frequency-shaped pulse outperforms the other pulses by having an APE gain of 0.628 dB compared to S2 pulse, the best previously known.

The algorithm does not put any constraints on the number of input parameters. However, increasing the frequency resolution results in a longer convergence time of the algorithm. If $\mathcal{Q}(f)$ is discretized into $\mathcal{N}$ points, the algorithm will vary only $\mathcal{N}-2$ points, leaving fixed the first and last points. The simulations were performed varying $\mathcal{N}$ from 7 to 130 points, achieving the best result for $\mathcal{N}=17$, shown in Fig. 5.5.

The fact that the best result is obtained for $\mathcal{N}=17$ does not match the common sense, higher the resolution, the better the result. Intuitively, increasing the frequency resolution $\mathcal{N}$ increases the chances of getting stuck into a local maximum. As mention in Sec. 4.3, the objective function is not concave and contains many local maxima. This work does not claim that the proposed pulse is globally optimal, but is the best out of this analysis. It must be noted that $\mathcal{N}=17$ is optimal in this study. However, in general the optimum value of $\mathcal{N}$ depends on initialization of the Nelder-Mead optimization.

In Fig. 5.5, the numerically optimized pulse in the frequency domain is compared

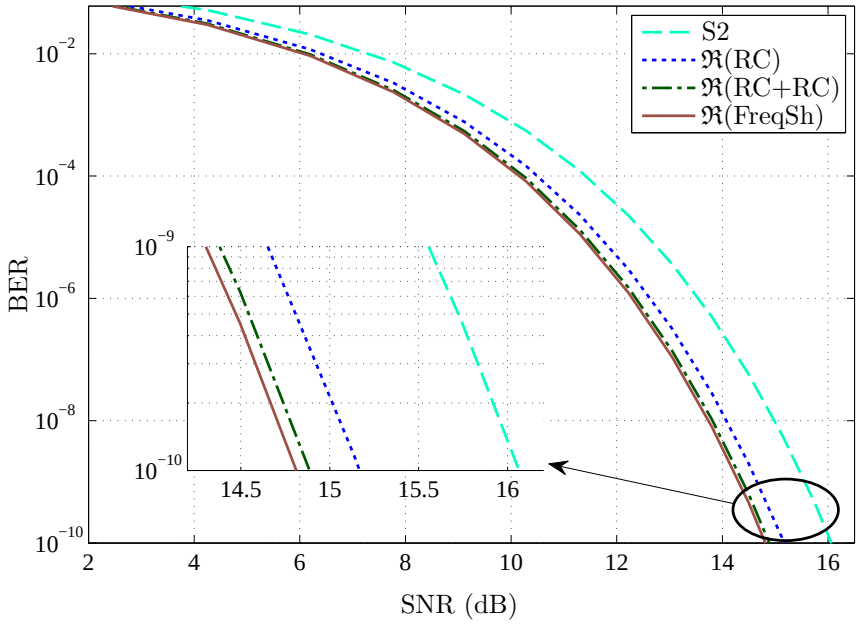

Figure 5.7. Pulses from Fig. 5.5 are analyzed in terms of BER as a function of SNR.

in the time domain with the S2 pulse and the best pulses previously obtained. The frequency-shaped pulse has the largest main lobe, almost of the same amplitude as the $\Re$(RC+RC) pulse. Comparing the decaying rate, the numerically optimized pulse in the frequency domain has noticeable smaller side lobes at $t = 4000\,T$ compared to the rest of the pulses.

The achievable APE gains for the pulses of Fig. 5.5 are shown in Fig. 5.6. The S2 pulse (the best previously known pulse) is outperfomed by means of the proposed variable-bias signaling and using an MF receiver. The frequency-shaped pulse has the best performance due to its better decaying rate, followed by the composite pulse.

Fig. 5.7 presents a different analysis by comparing the bit error rate (BER) as a function of the required signal-to-noise ratio (SNR) in terms of average optical power defined as in (Kahn and Barry 1997, Eq. (5))

$$\mathrm{SNR} = \frac{P_{\mathrm{opt}}^2}{N_0 R_b}, \tag{5.5}$$

where $R_b = 1/T$ is the bit rate.

The evaluated pulses preserve the same order as in Fig. 5.6 in terms of the performance. A gain of 1.26 dB is achieved between the proposed signaling method using the frequency shaped pulse and the best previously known scheme, which uses the S2 pulse.

6 Conclusion and Future Work

This thesis presents a new modulation format for IM/DD systems by designing a new bias signal and new bandlimited ISI-free pulses. The proposed bias signal is optimal for bandlimited transmission $B \leq 1/T$, consisting of a DC bias and a cosine term, being more power-efficient than the previously proposed pure DC bias. Moreover, new designs of Nyquist and root-Nyquist pulses are introduced, which further improve the power efficiency. The proposed method enables for the first time the power-efficient use of root-Nyquist pulses and the matched filter design at half the Nyquist rate. The evaluation of the new modulation formats is done by computing the asymptotic power efficiency, which shows gains up to 0.628 dB compared to the best previously known signaling method, which corresponds to 1.26 dB in terms of SNR.

6.1 Future Work

The results of this thesis point to several interesting directions for future work:

- Employing a different optimization algorithm than the one described in (Nelder and Mead 1965) in order to improve the final result.
- Design of composite pulses by combining more than two pulses.
- Analysis of the system performance in case of relaxing the nonnegativity constraint and employing error correction codes.
- The strict bandwidth limitation can be relaxed and the distorting effect of bandlimited hardware can be analyzed and mitigated using error correction codes.
- Analysis of other channel types, different from AWGN, which give good approximations for different applications.

Bibliography

Agrawal, G. P., (2005), *Lightwave Technology: Telecommunication Systems,* John Wiley & Sons Inc. Hoboken, NJ.

Anderson, J. B., (2005), *Digital Transmission Engineering,* 2nd ed. IEEE Press. Piscataway, NJ.

Barry, J. R., (1994), *Wireless Infrared Communications,* Kluwer Academic Publishers. Norwell, MA.

Beaulieu, N. C. and Damen, M. O., (2004), Parametric construction of Nyquist-I pulses, *IEEE Transactions on Communications*, **52**(12), pp. 2134–2142.

Beaulieu, N. C., Tan, C. C. and Damen, M. O., (2001), A 'better than' Nyquist pulse, *IEEE Communications Letters*, **5**(9), pp. 367–368.

Bouchet, O., Sizun, H., Boisrobert, C., de Fornel, F., and Favennec, P.-N., (2010), *Free-Space Optics, Propagation and Communication*, ISTE. Newport Beach, CA.

Hranilovic, S., (2005*a*), Minimum bandwidth Nyquist and root-Nyquist pulses for optical intensity channels, *IEEE Global Communications Conference,* vol. 3. pp. 1368–1372.

Hranilovic, S., (2005*b*), *Wireless Optical Communication Systems*, Springer. Boston, MA.

Hranilovic, S., (2007), Minimum-bandwidth optical intensity Nyquist pulses, *IEEE Transactions on Communications*, **55**(3), pp. 574–583.

Kahn, J. M. and Barry, J. R., (1997), Wireless infrared communications, *Proceedings of the IEEE*, **85**(2), pp. 265–298.

Kao, K. C. and Hockham, G. A., (1966), Dielectric-fibre surface waveguides for optical frequencies, *Proceedings of the Institution of Electrical Engineers*, **113**(7), pp. 1151–1158.

Molin, D., Kuyt, G., Bigot-Astruc, M. and Sillard, P., (2011), Recent advances in MMF technology for data networks, *Optical Fiber Communication Conference and Exposition and the National Fiber Optic Engineers Conference*, paper OWJ6.

Nelder, J. A. and Mead, R., (1965), A simplex method for function minimization, *The computer journal*, **7**(4), pp. 308–313.

Phillips, C. L., Parr, J. M. and Riskin, E. A., (2008), *Signals, Systems, and Transforms*, 4th ed. Prentice Hall. Upper Saddle River, NJ.

Proakis, J. G. and Salehi, M., (2008), *Digital Communications*, 5th ed. McGraw-Hill. New York, NY.

Randel, S., Breyer, F. and Lee, S. C. J., (2008), High-speed transmission over multimode optical fibers, *Conference on Optical Fiber Communication/National Fiber Optic Engineers*, paper OWR2.

Tan, C. C. and Beaulieu, N. C., (2004), Transmission properties of conjugate-root pulses, *IEEE Transactions on Communications*, **52**(4), pp. 553–558.

Tavan, M., Agrell, E. and Karout, J., (2012), Bandlimited intensity modulation, *IEEE Transactions on Communications*, **60**(11), pp. 3429–3439.

Westbergh, P., Gustavsson, J. S., Haglund, Å., Larsson, A., Hopfer, F., Fiol, G., Bimberg, D. and Joel, A., (2009), 32 Gbit/s multimode fibre transmission using high-speed, low current density 850 nm VCSEL, *Electronics Letters*, **45**(7), pp. 366–368.

Xia, X. G., (1997), A family of pulse-shaping filters with ISI-free matched and unmatched filter properties, *IEEE Transactions on Communications*, **45**(10), pp. 1157–1158.